

# Wake Fields in TESLA Accelerating Structures: Spectral Element Discontinuous Galerkin (SEDG) Simulations\*

Misun Min,<sup>†‡</sup> Paul F. Fischer,<sup>‡</sup> Yong-Chul Chae,<sup>§</sup>

<sup>‡</sup>Mathematics and Computer Science Division, Argonne National Laboratory, Argonne, IL 60439, USA

<sup>§</sup>Advanced Photon Source, Argonne National Laboratory, Argonne, IL 60439, USA

## Abstract

Using our recently developed high-order accurate Maxwell solver, NEKCEM, we carried out longitudinal wakefield calculations for a 9-cell TESLA cavity structure in 3D. Indirect method is used for wake potential calculations. Computational results with NEKCEM are compared with those of GdfidL.

## INTRODUCTION

NEKCEM uses a spectral element discontinuous Galerkin (SEDG) method based on a domain decomposition approach using spectral-element discretizations on Gauss-Lobatto-Legendre grids with body-conforming hexahedral meshes [1]. The numerical scheme is designed to ensure high-order spectral accuracy [2, 4], using the discontinuous Galerkin form with boundary conditions weakly enforced through a flux term between elements. Concerns related to implementation on wake potential calculations are discussed, and wake potential calculations with indirect method by NEKCEM [3] compared with the results of the finite difference time-domain code GdfidL.

## FORMULATIONS

The governing equations to study beam dynamics and numerical discretizations in space and time are described as follows.

### Maxwell's Equations

We begin with the Maxwell equations:

$$\mu \frac{\partial H}{\partial t} = -\nabla \times E, \quad \epsilon \frac{\partial E}{\partial t} = \nabla \times H - J \quad (1)$$

$$\nabla \cdot E = \frac{\rho}{\epsilon}, \quad \nabla \cdot H = 0, \quad (2)$$

where the current source  $J = (0, 0, J_z)$  is defined for an ultrarelativistic on-axis Gaussian beam moving in the  $z$ -direction:

$$J_z = c\rho(x, y)\rho(z - ct), \quad (3)$$

$$\rho(x, y) = \frac{1}{\sigma_r \sqrt{2\pi}} \exp\left(-\frac{x^2 + y^2}{2\sigma_r^2}\right), \quad (4)$$

$$\rho(z) = \frac{1}{\sigma_z \sqrt{2\pi}} \exp\left(-\frac{z^2}{2\sigma_z^2}\right). \quad (5)$$

\* Work supported by the U.S. Dept. of Energy under Contract DE-AC02-06CH11357.

<sup>†</sup> mmin@mcs.anl.gov

### Conservation Form

We rewrite equation (1) into a conservation form

$$Q \frac{\partial q}{\partial t} + \nabla \cdot F(q) = -J, \quad (6)$$

where

$$q = (H_x, H_y, H_z, E_x, E_y, E_z)^T, \quad (7)$$

$$Q = \text{diag}(\mu, \mu, \mu, \epsilon, \epsilon, \epsilon), \quad (8)$$

and the flux  $F(q)$  is defined in the following form:

$$\left[ \begin{array}{cccccc} 0 & E_z & -E_y & 0 & -H_z & H_y \\ -E_z & 0 & E_x & H_z & 0 & -H_x \\ E_y & -E_x & 0 & -H_y & H_x & 0 \end{array} \right]^T. \quad (9)$$

### Numerical Discretizations

We seek a numerical solution  $\mathbf{q}_N$ , satisfying

$$\left( Q \frac{\partial \mathbf{q}_N}{\partial t} + \nabla \cdot F(\mathbf{q}_N) + J, \phi \right)_{\Omega^e} = (\hat{n} \cdot [F - F^*], \phi)_{\partial\Omega^e}, \quad (10)$$

where  $\phi = L_i(x)$  is a local discontinuous test function and the numerical flux  $F^*$  is defined as in [2]. In the computational domain  $\Omega$  as a set of body-conforming, nonoverlapping hexahedral meshes  $\Omega^e$ , we define the local solution  $\mathbf{q}_N$  on each  $\Omega^e$  as

$$\mathbf{q}_N(x, t) = \sum_{j=0}^N q_j(t) L_j(x), \quad (11)$$

where  $q_j(t)$  is the solution at  $N$  grid points  $x_j$  on  $\Omega^e$ , and  $L_j(x)$  is the three-dimensional Legendre Lagrange interpolation polynomial associated with the  $N$  nodes [1]. Plugging (11) into the weak formulation (10) and taking Gauss quadrature for the integration, we obtain a semi-discrete formulation of the scheme. Then we apply the fourth-order Runge-Kutta method for time integration.

### Initial and Boundary Conditions

Initial fields are computed numerically for the ingoing pipe. For boundary conditions, we apply the uniaxial perfectly matched layer (UPML) [5] in the longitudinal direction and the perfectly electric conducting (PEC) boundary [2] in the transverse direction.

## COMPUTATIONAL RESULTS

We demonstrate a 9-cell TESLA mesh and its wake potentials for various bunch sizes at different radii. Results are compared to GdfidL for the bunch size  $\sigma_z = 5$  mm. Parallel efficiency of NEKCEM is also discussed.

### TESLA Cavity with a Spectral-Element Mesh

We built a 9-cell TESLA mesh shown in Figure 1, following [6]. In the transverse direction, we scale meshes for a radius greater than  $r = R$  mm (Figure 1 shows the case  $r = 15$  mm). Then we compute wake potentials along the mesh surface at  $r = R$  in three dimensions.

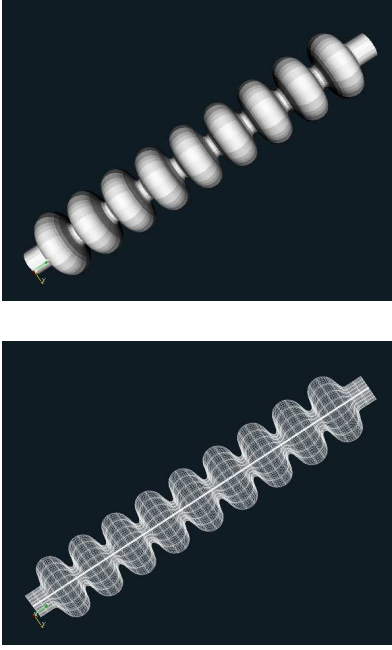


Figure 1: 9-cell TESLA mesh (top); spectral-element discretization (bottom).

### Wake Potential

We compute the longitudinal wake potential defined as

$$W_z(x, y, s) = -\frac{1}{Q} \int_{-\infty}^{\infty} E_z(x, y, z, t) dz, \quad (12)$$

where  $Q$  is the total charge of a beam and  $s = ct - z$ . Then we obtain wake potential at  $r = R$  from defining

$$W_z^1(s) = \frac{1}{2\pi R} \int_{\partial\Omega_R} W_z(x, y, s) dx dy, \quad (13)$$

where  $\partial\Omega_R$  represents the surface at  $r = R$ .

Figure 2 shows wake potentials for different bunch sizes with a fixed polynomial degree  $N = 5$  and the number of elements  $E = 1,368$ . The behaviors of the wake potential profiles show reasonable profiles for bunch sizes 3 mm, 4 mm, and 5 mm.

Since we use an indirect method for our wake potential calculations, we examine how the wake potential profiles change at different radii. Figure 3 shows wake potential profiles at radius 26.0 mm and radius 19.25 mm for bunch size 5 mm with polynomial degree,  $N = 5$  and number of element  $E = 1,368$ . A discrepancy for these cases at radii 26.0 mm and 19.25 mm is observed on the unstructured grids, unlike the case for the finite difference grids. Further study is needed with relatively even and finer meshes for the unstructured mesh case.

Figure 4 compared GdfidL and SEDG for the wake potentials with bunch size 5 mm. For SEDG, the dashed line shows the case for  $N = 7$  and solid line for  $N = 5$ . A discrepancy is observed in the results of GdfidL and SEDG. Further study must be carried out with different meshes and resolutions for the unstructured mesh case.

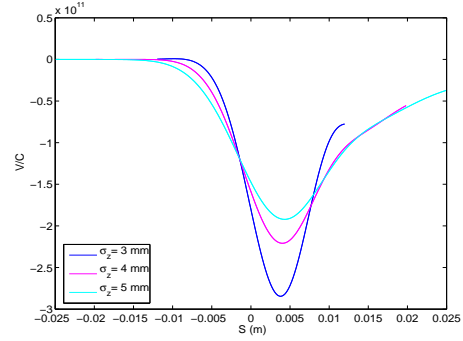


Figure 2: Wake potentials on the surface at  $r = 26.0$  mm for  $\sigma_z = 3$  mm, 4 mm, and 5 mm and  $\sigma_r = 1$  mm.

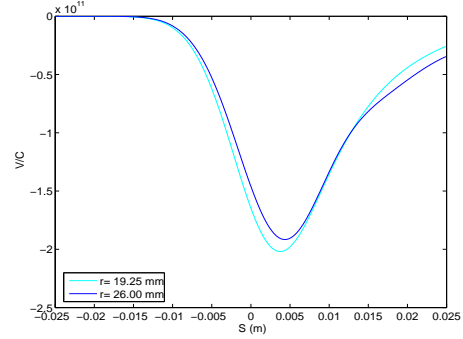


Figure 3: Wake potentials on the surface at  $r = 26.0$  mm and  $r = 19.25$  mm for  $\sigma_z = 5$  mm and  $\sigma_r = 1$  mm.

### Parallel Efficiency

Figure 5 shows the scaling of 3D computations of NEKCEM. The vertical axis is CPU time per time step, per grid point, per processor. The number of elements is fixed at  $E = 512$  ( $8^3$ ). The polynomial degrees vary from  $N = 5$  to 10. Simulations were run on Argonne's Linux cluster, Jazz, with processors  $P = 2^k$ ,  $k = 0, \dots, 7$ . The coarsest computations involve  $n = 64,000$  points, which

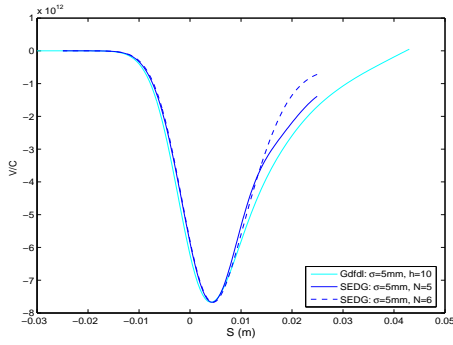


Figure 4: Wake potentials on the surface at  $r = 26.0\text{mm}$  for  $\sigma_z = 5\text{ mm}$  and  $\sigma_r = 1\text{ mm}$  on the meshes.

yield roughly 100 points per processor for  $P = 128$ . Each curve shows some loss of parallel efficiency as the number of processors is increased: the CPU time increases from right ( $P = 1$ ) to left ( $P = 128$ ) on the graph. Below approximately 3,000 to 10,000 points per processor, the CPU time actually *decreases* with superlinear speedup.

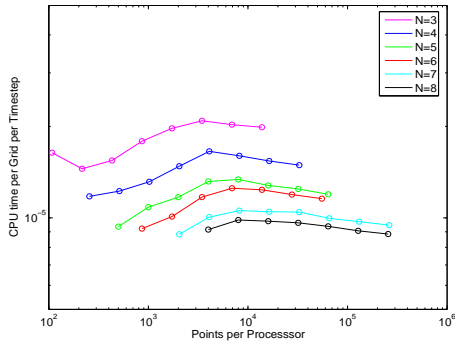


Figure 5: CPU time per grid point per time step per processor for 512 spectral elements with  $N$  ranging from 5 to 10, as a function of number of points per processor on Jazz.

## CONCLUSIONS

We have applied the spectral-element discontinuous Galerkin method to simulate beam dynamics within a three-dimensional 9-cell TESLA cavity. The wake potential calculations show resonable profiles depending on the bunch size. We compared the wake potential calculations with GdfidL results. We observe some discrepancy in the wake potential profiles of SEDG compared to the cases in GdfidL. Further study will be carried out regarding the mesh refinement and resolution as a first step toward one-picosecond bunch simulations.

## REFERENCES

[1] M.O. Deville, P.F. Fischer, and E.H. Mund, “High Order Methods for Incompressible Fluid Flow,” Cambridge University Press (2002).

[2] J.S. Hesthaven and T. Warburton, “Nodal High Order Methods on Unstructured Grids - I: Time-Domain Solution of Maxwell’s Equations,” J. Comp. Physics, 101 (2002), p. 186.

[3] M.S. Min and P.F. Fischer, “NEKCEM,” Mathematics and Computer Science Division, Argonne National Laboratory. <http://mercurial.mcs.anl.gov/nekcem/>.

[4] M.S. Min, P.F. Fischer, and Y.C. Chae, “Spectral element discontinuous Galerkin simulations for wake potential calculations: NEKCEM,” Proc. of Particle Accelerator Conference, 2007.

[5] A. Taflov and S.C. Hagness, “Computational Electromagnetics: The Finite-Difference Time Domain Method,” Artech House, 3rd ed. (2005).

[6] R. Wanzenburg, “Monopole, Dipole and Quadrupole Passbands of the TESLA 9-cell Cavity,” TESLA 2001-33, DESY, 2001.

The submitted manuscript has been created by UChicago Argonne, LLC, operator of Argonne National Laboratory (“Argonne”). Argonne, a U.S. Dept. of Energy Office of Science laboratory, is operated under Contract DE-AC02-06CH11357. The U.S. Government retains for itself, and others acting on its behalf, a paid-up, nonexclusive, irrevocable worldwide license in said article to reproduce, prepare derivative works, distribute copies to the public, and perform publicly and display publicly, by or on behalf of the Government.